Turk J Chem
35 (2011) , 881 – 891.

doi:10.3906/kim-1102-989

Synthesis and structural analysis of a regular Cu-Mg-Al hydrotalcite-like compound

Jian-Song WU[1,*], Ying-Kai XIAO[2], Yu-Ping LIU[1], Wan-Bang XU[3], Mei-Fang LIANG[1], Jian CHENG[1], Jian-Ping WAN[1], Ling-Zhu CHEN[1]

[1] *School of Chemistry Science and Technology, Zhanjiang Normal College, 524048, Zhanjiang-CHINA*
e-mail: wujs1976@yahoo.com.cn

[2] *Key Laboratory of Salt Lake Resources and Chemistry, Qinghai Institute of Salt Lakes, Chinese Academy of Sciences, 810008, Xining-CHINA*

[3] *Guangdong Institute for Drug Control, 510180 Guangzhou-CHINA*

Received: 22.02.2011

A fine-quality, regular Cu-Mg-Al hydrotalcite-like compound was synthesized via the glycothermal method using $CuCl_2 \cdot 2H_2O$, $MgCl_2 \cdot 6H_2O$, $AlCl_3 \cdot 6H_2O$, and Na_2CO_3 as raw materials and sodium hydroxide as the precipitant. Hydrotalcite samples were characterized by X-ray diffraction, scanning electron microscopy, transmission electron microscopy, Fourier transform infrared spectroscopy, thermogravimetric-differential thermal analysis, and Brunauer-Emmett-Teller N_2 surface area measurements. The influence of glycol content on the characteristics of the sample was investigated. The results show that the glycol content in the system had a greater impact on regular hydrotalcite with an intercalated structure. A Cu-Mg-Al hydrotalcite-like compound with a well-defined shape, distinct intercalated structure, regular quality, and good dispersing capability could be obtained under the following conditions: glycol volume ratio of 10%, hydrothermal temperature of 180 °C, and reaction time of 15 h. The compound obtained was well crystallized and had the morphology of a homogeneous and hexagonal sheet. The thickness of each hexagon in the hydrotalcite was about 40 nm, which was consistent with the value estimated with the Scherer equation.

Key Words: Glycol, hydrothermal, Cu-Mg-Al hydrotalcite-like compound, synthesis structural analysis

Introduction

Hydrotalcite-like compounds (HTlcs) are an important class of inorganic functional materials because of their special layered structure. HTlcs have the general formula of $[M^{2+}_{1-x}M^{3+}_x(OH)_2]^{x+}(A^{n-}_{x/n}) \cdot mH_2O$, where M^{2+}

*Corresponding author

is a divalent cation (Mg^{2+}, Cu^{2+}, etc.), M^{3+} is a trivalent ion ($A1^{3+}$, Fe^{3+}, etc.), and $A^{n-}_{x/n}$ is the gallery anion. The space group of HTlcs belongs to $P\bar{3}^{-}m_1$, a= 0.3070 nm, c = 2.23 nm. Figure 1 schematically illustrates the layer structure of HTlcs, and Figure 2 illustrates the unit cell of HTlcs.

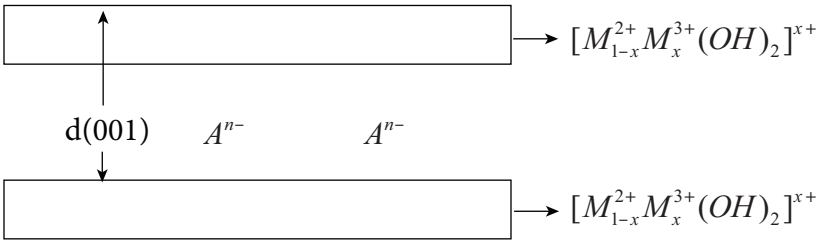

Figure 1. HTlc layer structure.

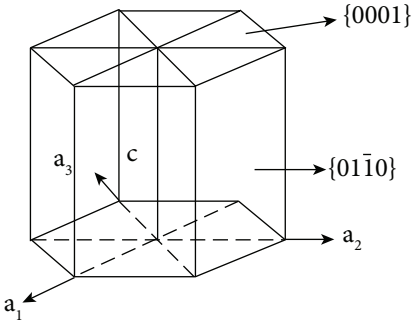

Figure 2. The unit cell of HTlcs.

HTlcs have good potential in areas such as catalysis, flame retardation, absorption, medicine, and gene storage.[1−5] The Cu-Mg-Al HTlc is one of the most important HTlcs. Cu HTlcs catalyze hydroxylation and hydrogenation.[6−8] In the synthesis of Cu-Mg-Al HTlcs, the Mg^{2+} in the magnesium hydroxide is partially substituted by Cu^{2+} and Al^{3+} to form derivatives. Thus, its structure is similar to the layered structure of magnesium hydroxide. Hydrotalcite, with its fine dispersive character and regular shape, has superior function and has been used in industrial production in various countries. The layered structure, regular shape, granular distribution, and dispersive character of hydrotalcite influence its applicability.[9−11] The traditional method for preparation of HTlcs is liquid-phase deposition, wherein the crystal growth of the product is less ordered and does not significantly form hexagonal sheets.[12−14] Kim et al.[15] prepared a Mg-Al hydrotalcite film by electrophoretic deposition. Taibi et al.[16] prepared Ni-Fe hydrotalcite using polyol alkoxide in a polyalcohol medium. These methods are different from the conventional precipitation method. There has still not been a significant improvement in the dispersion and regularity of hydrotalcite products. Guangdong salt brine and Qinghai salt lake brine are rich magnesium resources. Therefore, designing new technology to utilize these high-quality magnesium resources and prepare high-quality magnesium copper hydrotalcite is necessary. The glycothermal method is a new technique designed in this work. A thin layer of Cu-Mg-Al HTlc with regular morphology, good crystal shape, uniform size, and good dispersion was successfully prepared. The process involved a hydrothermal reaction system containing a certain amount of glycol, whose influence on hydrotalcite crystal growth was examined. The Cu-Mg-Al-HTlc crystal structure was also analyzed.

Experimental

Preparation of the Cu-Mg-Al-HTlc sample

The main equipment for the synthesis was a quick-change stirred autoclave (KCF-10, Optical Precision Instrument Factory, Yantai Muping Shu, China). All reagents used were of analytical grade.

Various glycol solutions with 0%, 5%, 10%, 15%, and 20% volume fractions of glycol, marked as Samples 1 through 5, respectively, were prepared. Solutions of 0.6 mol L^{-1} $CuCl_2 \cdot 2H_2O$, 0.6 mol L^{-1} $MgCl_2 \cdot 6H_2O$, 0.4 mol L^{-1} $AlCl_3 \cdot 6H_2O$, and 0.2 mol L^{-1} Na_2CO_3 were prepared using the glycol solutions as diluents. A solution of $[n(Cu^{2+}):n(Mg^{2+}):n(Al^{3+}):n(CO_3^{2+}) = 3:3:2:1]$ was prepared by combining the above solutions under slow stirring. The pH of the solutions was adjusted to approximately 12 using 6 mol L^{-1} of NaOH solution. Finally, a milky white slurry was obtained. The reaction started when 1500 mL of the milky white slurry was loaded into the autoclave, set at 180 °C with a stirring speed of 300 circles/min. The reaction was finished after 15 h. The sediment produced was filtered and washed with distilled water until the filtrate was near neutral. The sediment was placed in the oven (70 °C) to receive the sample. Recovery of glycol was done by distillation.

Instruments for phase, morphology, surface area, thermal, and structural analyses of Cu-Mg-Al HTlc

The instruments for phase, morphology, surface area, thermal, and structural analyses were as follows. For X-ray diffraction (XRD), a D/Max-3C diffractometer (Rigaku, copper target, graphite curved-crystal monochromator), set at a scanning rate of 3° min^{-1} and a scan range of 10-70°, was used. For determination of Cu, Mg, and Al, an Ultima plasma emission spectrometer (JY Company, France) was used. Determination of C and H was done with a PE 2400 Series II CHNS/O elemental analyzer (PerkinElmer, USA). A Philips SL-30 scanning electron microscope and JEM-200CX transmission electron microscope (Japan Electronics Co., Ltd.) were used for morphology analysis. Fourier transform infrared spectroscopy (FTIR) was performed using a Magna 550 (II) FTIR spectrophotometer (Nicolet, USA). An AsAp 2010 surface area/gap analysis instrument (Micromeritics Company, USA) was used for surface area analysis. The samples were subjected to 80 °C and 2.7 Pa pretreatment, and were then held under vacuum for 8 h at 0.4 Pa to determine the surface area/gap distribution.

Results and discussion

Cu-Mg-Al-HTlc phase analysis and cell structure analysis

Figure 3 shows the X-ray diffraction models of the 5 samples. To confirm the Cu-Mg-Al-HTlc samples, we compared these models with the results of Mg-Al hydrotalcite quasi-diffraction (JCPDS file number 14-0191). The patterns of the 5 samples were identical in relative signal strength and standard diffraction profile. We inputted the diffraction data of each sample into Origin 7.5 software to calculate the half-peak width for (003): Sample 1 at 0.76°, Sample 2 at 0.81°, Sample 3 at 0.30°, Sample 4 at 0.53°, and Sample 5 at 0.62°.

The sharpest diffraction peak of Sample 3 for the (003), (006), and (009) planes proves that it had the best crystallinity. The crystallinities of Samples 1, 2, 4, and 5 were relatively poor. The order of crystallinity of the 5 samples was as follows: Sample 3 > Sample 2 ≈ Sample 4 > Sample 1 ≈ Sample 5. Table 1 lists the maximum diffraction intensity and the corresponding d values of the 5 samples for the (003), (006), and (009) crystal planes. From Table 1, the d_{003} value of Sample 3 is seen to be twice its d_{006} value and thrice its d_{009} value. These findings show that Sample 3 had a very neat board, whereas the multiple relationships for the other 4 samples were relatively poor. Thus, we could determine the minimum half-peak width of Sample 3 based on the diffraction intensity. The crystallinity of Sample 3 was highest and that of Sample 1 was lowest.

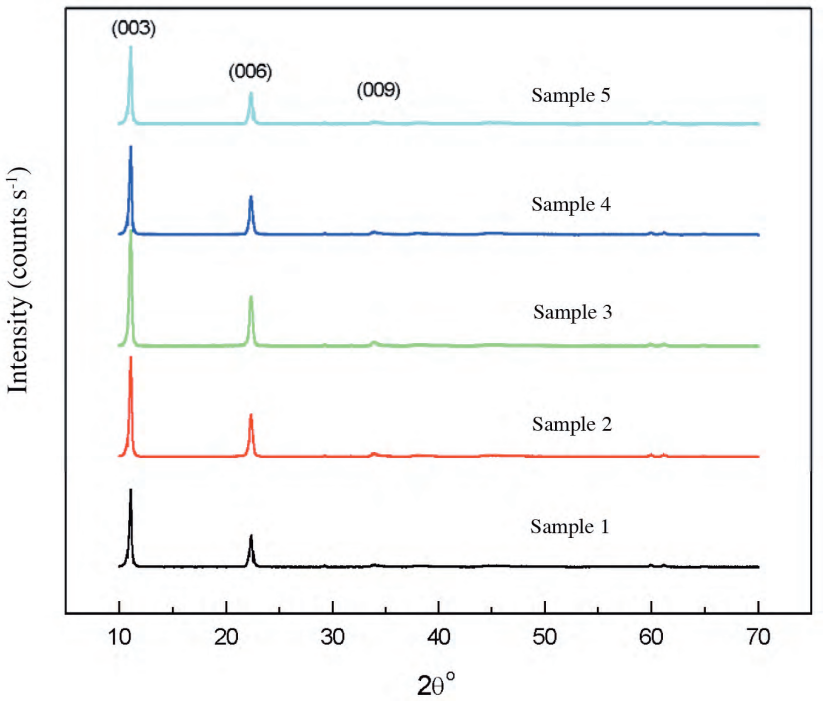

Figure 3. The XRD patterns of the samples.

Table 1. XRD patterns of samples.

Sample	(003)		(006)		(009)	
	$2\theta_{003}$ (°)	d_{003} (nm)	$2\theta_{006}$ (°)	d_{006} (nm)	$2\theta_{009}$ (°)	d_{009} (nm)
1	11.01	0.8026	22.11	0.4015	33.58	0.2666
2	11.05	0.7997	22.23	0.3994	33.45	0.2675
3	11.04	0.8004	22.22	0.4001	33.58	0.2666
4	11.03	0.8012	22.24	0.3992	33.56	0.2665
5	11.09	0.7968	22.26	0.3964	33.43	0.2677
JCPDS	14.47	0.6113	28.91	0.3084	44.10	0.2051

According to the literature,[1,17,18] the a and c values of each sample cell can be calculated based on the numerical value of the diffraction and the d value. The interlayer channel height h can then be obtained by subtracting the spacing (about 0.477 nm) from the layer thickness.[1,18] The particle size can be estimated according to the XieLe formula: $Q = \frac{0.89\lambda}{\beta \cdot \cos\theta} \cdot \frac{180}{\pi}$ (Q: size of particle, β: half-peak width, λ: X-ray wavelength, θ: Bragg angle). The calculated results are listed in Table 2, showing that the a values and particle sizes decreased from Samples 1 to 3, but increased from Samples 3 to 5. All c and h values decreased from Samples 1 to 5; this indicates that the increased glycol content in the reaction system decreased the lamellar spacing and channel height. The increase in the glycol concentration from 0% to 10% (v/v) could decrease the octagonal electrostatic repulsion of $[\text{Cu-O}_6]^{10-} \cdot [\text{Mg-O}_6]^{10-} \cdot [\text{Al-O}_6]^{9-}$. Thus, the a value and particle size decreased. However, when the concentration of glycol was higher than 10%, the growth of the composite octagonal repulsion had a major effect, resulting in an increase in the a value and the particle size. The c and h values were closely related to the crystal growth medium.[19] Glycol is a small molecule and can form a hydrogen-bonded network, which differs from that in water. Glycol has high cohesion and a high boiling point (198 °C). These characteristics make the growth characteristics of the octahedron in the mixed system of glycol different from those in pure water. The increase in glycol concentration caused the c and h values to decrease. The octagonal growth mechanism from the hydrogen network formed by glycol and water needs to be studied further.

Table 2. Analysis results of Cu-Mg-Al-HTlc lattice parameters.

Sample	Lattice parameter (nm)			Particle size (nm)
	a	c	h	
1	0.3075	2.405	0.3247	38.25
2	0.3061	2.401	0.3233	36.45
3	0.3039	2.400	0.3230	32.14
4	0.3085	2.399	0.3227	33.87
5	0.3089	2.393	0.3207	33.96

Table 3 lists the element analysis results of the 5 samples. The data in Table 3 show that Sample 3 had a composition of $n_{Cu}:n_{Mg}:n_{Al}:n_C = 3:3:2:1$. The pattern of $Cu_3Mg_3Al_2(OH)_{16}CO_3 \cdot 4H_2O$ can be roughly inferred combined with the oxygen content (obtained by difference) and hydrogen content. Its pattern accords with those of HTlcs. However, Samples 1, 2, 4, and 5 showed deviations. The Cu content was low, which may be because of the difficulty involved in incorporating Cu^{2+} into the grid matrix at low glycol contents. The mass of $[\text{Mg-O}_6]^{10-}$ is greater than that of $[\text{Mg-O}_6]^{10-} \cdot [\text{Al-O}_6]^{9-}$. The Cu fraction in the pure water system cannot enter the crystalline structure due to its strong polarity. Collision probability is therefore lower in the pure water system. When the amount of glycol in the system is 10%, the polarity is reduced, which results in an apparent increase in content.

Morphological analysis of Cu-Mg-Al HTlc

The transmission electron microscopy (TEM) images of Samples 1-5 are shown in Figures 4a-4e, respectively. Figure 4a shows that the particles were clumped together, poorly dispersed, ambiguous in appearance, and

lacking distinct particle edges. Figure 4b shows that the particles were dispersed and had a grain shape and distinct edges, but they were still not ideal as a whole. Figure 4c shows that Sample 3 possessed fine dispersion, while the integrity of the hexagon was crystal-shaped, clean cut, had good morphology, and was structured. The estimated particle diameter, based on the electron micrographs, was about 40 nm, which was close to the values estimated from the XieLe formula. The dispersion, particle edges, and morphology of Sample 4 (Figure 4d) were poorer than those of Sample 3, and Sample 5 showed the worst morphology. Particle quality began to decline when the content of glycol was higher than 15%. Figure 5 shows the scanning electron microscopy (SEM) image of Sample 6, containing 40% glycol (a TEM image was not obtained because the sample particle was too thick for transmission). Figure 6 shows the SEM image of Sample 7, containing 60% glycol content (also too thick for a TEM image). The 2 images indicate that the quality of both Sample 6 and 7 was inferior.

Table 3. Element analysis results of Cu-Mg-Al HTlc.

Sample	ω (Cu)%	ω (Mg)%	ω (Al)%	ω(C)%	ω(H)%	Cu:Mg:Al:C molar ratio in samples
1	24.86	10.08	7.02	1.78	3.41	0.388:0.420:0.260:0.140
2	26.03	10.11	7.28	1.76	3.55	0.407:0.421:0.269:0.147
3	26.43	9.98	7.49	1.69	3.63	0.413:0.416:0.277:0.141
4	25.99	9.01	7.52	1.79	3.93	0.406:0.375:0.279:0.149
5	25.03	11.25	6.89	1.73	3.83	0.391:0.469:0.255:0.144

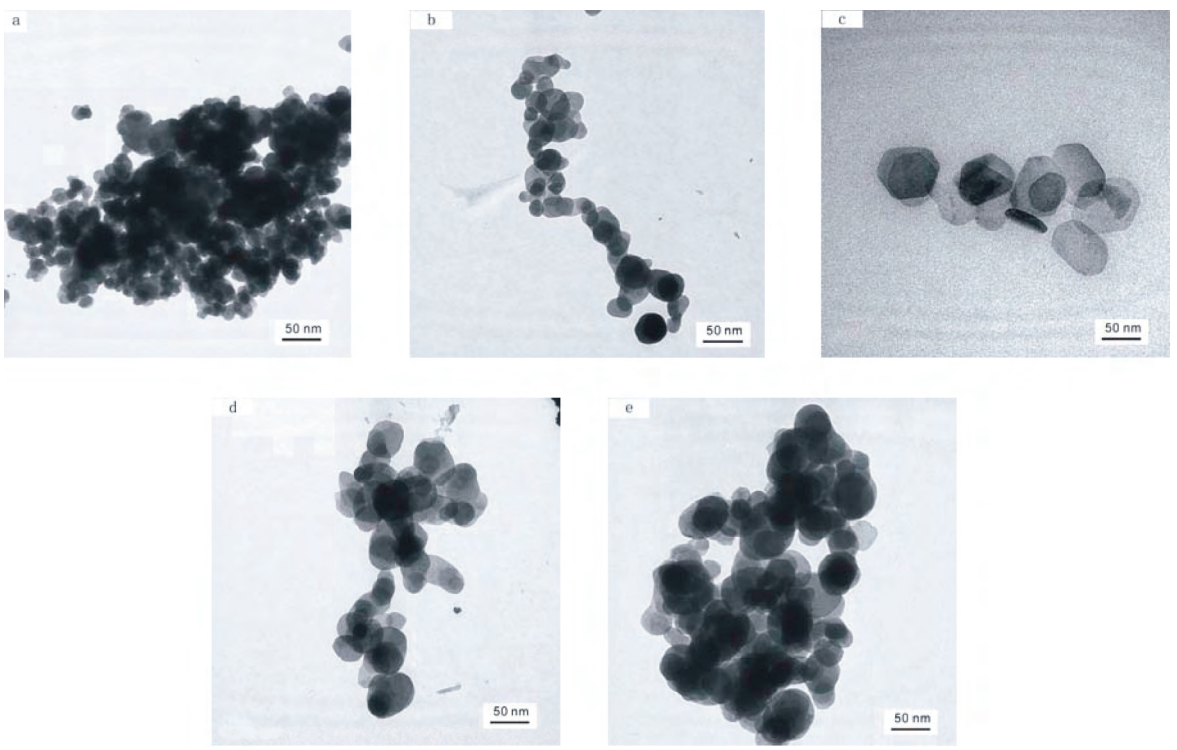

Figure 4. The TEM images of Samples 1 (a), 2 (b), 3 (c), 4 (d), and 5 (e).

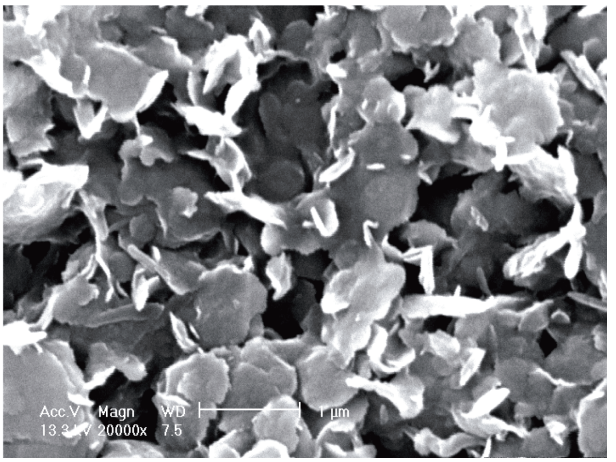

Figure 5. The SEM image of Sample 6.

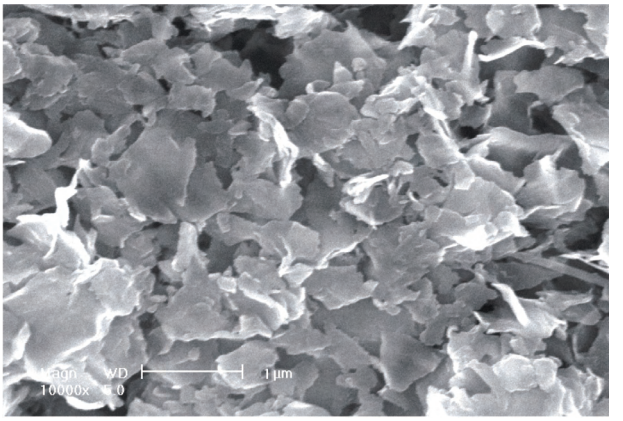

Figure 6. The SEM image of Sample 7.

FTIR spectroscopy of Cu-Mg-Al-HTlc

Figure 7 shows the FTIR spectra of the samples. The peak shapes (at 3800-3000 cm^{-1}) of samples containing different glycol contents varied. Samples 1 and 2 appeared to have sharp absorption at 3723 cm^{-1}; this suggests the disordered arrangement of water molecules and low symmetry. The double absorption band at 1750-1250 cm^{-1} for Samples 1, 2, 4, and 5 was caused by the significant asymmetry of CO_3^{2-}. This dual band was much less intense in the spectrum of Sample 2 than in the spectrum of Sample 1. Sample 3 did not give rise to such a band. This suggests that the glycol content of 0%-10% could be used to improve the ordering process. Therefore, the FTIR characterization of the hydrotalcite structure reflects the coexistence of a strong bond with a weak bond. The increase in bond strength between layers increased with crystallinity; this is consistent with the XRD diffraction model results and reflects the increase in the water-ordered lamellar structure. The asymmetric methylene stretching near 2926 cm^{-1} and the hydrocarbon asymmetric stretching near 2960 cm^{-1} were not found in the spectra. Therefore, the samples with high purity did not contain glycol. The maximum residual glycol (mass fraction) measured by spectrophotometry was 1.22×10^{-6}%.

Thermogravimetric-differential thermal analysis (TG-DTA) of Cu-Mg-Al HTlc

Figure 8 shows the TG-DTA thermogram for Sample 3. The TG curve shows 2 distinct weight-loss steps. The first mass-loss level of 9.63% was close to the theoretical value corresponding to the loss of crystal water, indicating that the main weight-loss phase involved in this step was the removal of interlayer water. The DTA endothermic peak corresponded to 148.63 °C. The decrease in the temperature for removal of the interlayer water (corresponding to the endothermic peak) indicates that the higher ordering of hydrotalcite samples resulted from a decreased effect of water molecules (crystal water) and lower, irregular hydration of metal ions. The second weight loss was 20.50%, which was closely related to the total content of the hydroxyl that underwent dehydration and the CO_2 released from CO_3^{2-}. This confirms that the second weight loss was mainly characterized by the destruction of the laminate structure. The characteristic endothermic DTA peak of the second phase split into 2 peaks: the first at 341.28 °C and another at 386.55 °C. These show that hydroxyl and CO_3^{2-} escaped stepwise.

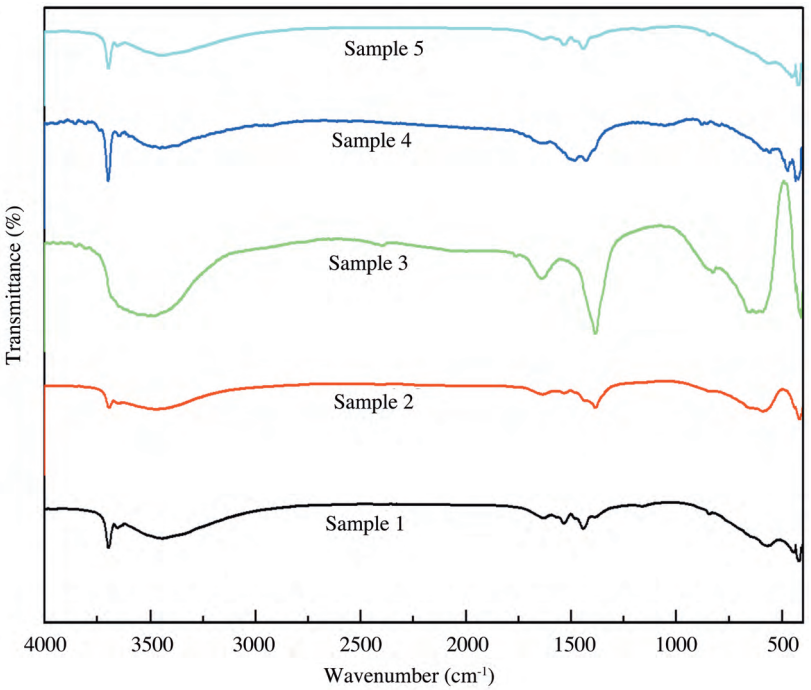

Figure 7. The FTIR spectra of the samples.

Based on the anionic coordination polyhedron growth unit model,[17,19] there is a hydroxyl hydrogen-forming bridge bond on the common edges of octahedral $M(OH)_6^{4-/3-}$ (M is the metal ion). This hydrogen atom is unstable and acidic. Therefore, the interlayer OH^- was first removed in the form of H_2O. CO_3^{2-} releases CO_2 at higher temperatures, which reflects the fact that the thermal stability of the Cu-Mg-Al-HTlc laminates significantly depend on their structural regularity. This is very consistent with the results reported by Gou et al.[20] The total mass loss of the thermal decomposition samples was 34.01%, which was close to the total mass loss of 36.01% calculated from the 2 stages of mass loss of 9.97% and 26.04% for the Cu-Mg-Al-HTlc formula, $Cu_3Mg_3Al_2(OH)_{16}CO_3 \cdot 4H_2O$. The changes of the TG-DTA curves at different temperatures reveal the coexistence of 2 structural levels, the group between layers and the broad and strong bond group in the Cu-Mg-Al-HTlc structural unit of the middle layer. The supramolecular structural features of Cu-Mg-Al HTlc were characterized by their thermodynamic properties. Thermal analysis further showed that the samples had high crystallinity and a significant layer structure.

Relative surface analysis of Cu-Mg-Al HTlc

Figure 9 shows the adsorption isotherms of Sample 3. Adsorption slowly increased in the first half of the isotherm, and then adsorption capacity rapidly increased in the second half. The shape was consistent with type-II adsorption characteristics. The loop of adsorption indicated capillary condensation and the presence of a sample with a hole of more than 5 nm. The pore size distribution was 0-10 nm for samples containing 8% glycol, 10-20 nm for 75%, and >20 nm for 17%; the average pore size was 15.1 nm. The desorption isotherms with

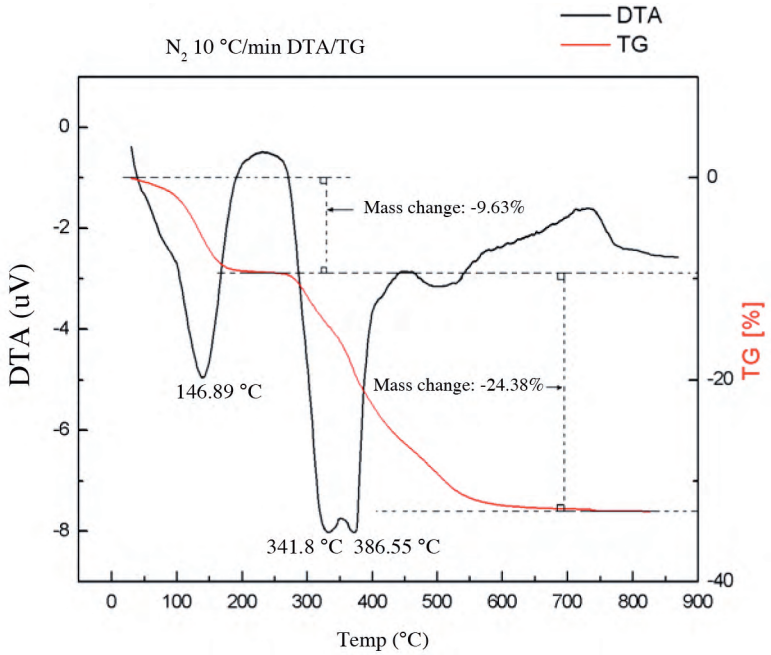

Figure 8. The TG-DTA patterns of Sample 3.

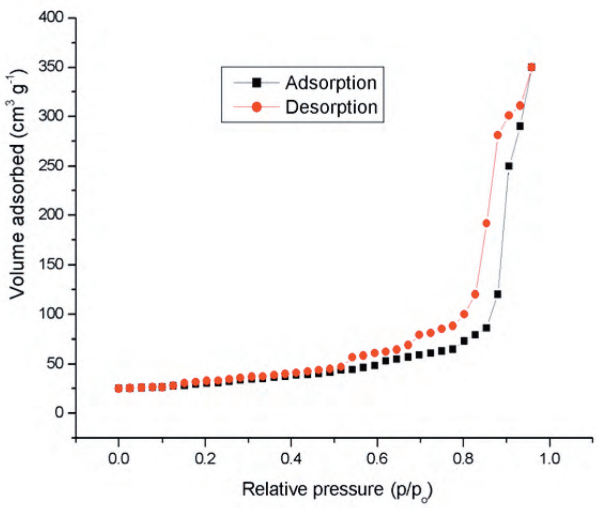

Figure 9. The isotherm of Sample 3.

a lagging loop at high pressure showed that sample adsorption was mainly due to pores with small diameters. The presence of channel micropores in the inner part of the Cu-Mg-Al-HTlc crystal was revealed by adsorption and desorption isotherms. A part of the adsorption was caused by the channel porous layer. The surface area increased with the high order of internal structure, uniform arrangement of interlayer carbonate ion columns, increase in channel pore density, and reduction in pore size. The S_{BET} value was approximately 136.92 $m^2 g^{-1}$.

Conclusion

High-quality Cu-Mg-Al HTlc, prepared by adding ethylene glycol to the hydrothermal system, has good regularity, significant lamellar structure, good crystal shape, good dispersion, high channel pore density with small apertures, and large surface area. Our conclusions are as follows.

First, the volume fraction of ethylene glycol in the hydrothermal system has a significant influence on crystallinity, regularity, and crystal shape, and has a slight influence on the lattice parameters (a, b, and c) of Cu-Mg-Al HTlc. Variations of lattice parameters caused by changes in the concentration of ethylene glycol were observed.

Second, high-quality Cu-Mg-Al HTlcs with well-defined shape, distinct intercalated structure, regular quality, and good dispersing capability can be obtained when the volume fraction of ethylene glycol in the reaction system is 10%. The unique characteristics of high-quality Cu-Mg-Al HTlc are as follows: the role of crystal water is small, the irregular hydration of metal ions is low, the adsorption isotherm accords with type-II behavior, and pores of >5 nm in diameter occur in the interlayer of the crystal.

Third, under certain conditions, ethylene glycol may coordinate with anionic polyhedron growth units $[\text{Cu-O}_6]^{10-}$, $[\text{Mg-O}_6]^{10-}$, and $[\text{Al-O}_6]^{9-}$ in the solution, and its concentration affects the centralization, nucleation speed, anisotropy, and growth velocity of the crystal.

Acknowledgment

This work was supported by the National Natural Science Foundation of China, Grant No. 40976074.

References

1. Liu, Y. H.; Guo, Y. H.; Wu, J. Y.; Liu, L. Y.; He, J.; Chen, B. H.; Pu, M. *Chem. J. Chinese U.* **2008,** *29*, 1171-1175.
2. Zhang, W. F.; Li, D. Q.; Sun, M.; Evans, D. G.; Duan, X. *Chem. J. Chinese U.* **2004,** *25*, 1799-1803.
3. Ren, L. L.; He, J.; Evans, D. G.; Duan, X. *Chem. J. Chinese U.* **2003,** *24*, 169-173.
4. Gou, G. J.; Ma, P. H.; Chu, M. X. *Chem. J. Chinese U.* **2005,** *26*, 497-502.
5. Cheng, J.; Yu, J. J.; Wang, X. P.; Li, L. D.; Li, J. J.; Hao Z. P. *Energy Fuel.* **2008,** *22*, 2131-2137.
6. Auer, S. M.; Gredig, S. V.; Köppel, R. A.; Baiker, A. *J. Mol. Catal. A Chem.* **1999,** *141*, 193-203.
7. Feng, Y. J.; Li, D. Q.; Li, C. X.; Wang, Z. G.; Evans, D. G.; Duan, X. *Acta Chim. Sinica* **2003,** *61*, 78-83.
8. Zhu, K. W.; Liu, C. B.; Ye, X. K.; Wu, Y. *Chem. J. Chinese U.* **1997,** *18*, 1530-1533.
9. Meng, J. H.; Zhang, H.; Evans, D. G.; Duan, X. *Chem. J. Chinese U.* **2003,** *24*, 1315-1319.
10. Zheng, J. H.; Tian, X. K.; Yu, K. C.; Wang, L. Y.; Yang, C.; He, M. Z. *Acta Chim. Sinica* **2006,** *64*, 2231-2234.
11. Luo, Q. S.; Li, L.; Wang, Z. X.; Duan, X. *Chinese J. Inorganic Chem.* **2001,** *17*, 835-842.
12. Zhao, R. Y.; Dang, C. L.; Zhao, H. J.; Liu, C. G. *Univ. Petr. (Nat. Sci. Ed.)* **2003**, *27*, 93-97.
13. Ren, Q. L.; Chen, W.; Luo, Q. *Chinese J. Inorganic Chem.* **2004**, *19*, 977-984.
14. Makoto, O.; Shiho, A. *Chem. Mater.* **2000**, *12*, 3253-3255.

15. Kim, T.; Sahimi, M.; Tsotsis, T. T.,*Ind. Eng. Chem. Res.* **2008**, *47*, 9127-9132.
16. Taibi, M.; Ammar, S.; Schoenstein, F.; Jouini, N.; Fievet, F.; Chauveau, T.; Greneche, J. M. *J. Phys. Chem. Solids* **2008**, *69*, 1052-1055.
17. Jiang, P.; Hou, W. G.; Han, S. H.; Hu, J. F.; Li, D. Q. *Chem. J. Chinese U.* **2002,** *23*, 78-82.
18. Constantino, V. R. L.; Pinnavaia, T. J. *J. Inorg. Chem.* **1995**, *34*, 883-892.
19. Zhang, X. H.; Luo, H. S.; Zhong, W. Z. *Sci. China. Ser. E* **2004**, *34*, 241-253.
20. Gou, G. J.; Ma, P. H.; Chu, M. X. *Acta Chim. Sinica* **2004**, *62*, 2150-2160.